

# Episodic deposition and $^{137}\text{Cs}$ immobility in Skan Bay sediments: A ten-year $^{210}\text{Pb}$ and $^{137}\text{Cs}$ time series

Susan F. Sugai<sup>a</sup>, Marc J. Alperin<sup>b</sup> and William S. Reeburgh<sup>c</sup>

<sup>a</sup>*Institute of Marine Science, University of Alaska, Fairbanks, AK 99775-1080, USA*

<sup>b</sup>*Curriculum in Marine Sciences, University of North Carolina, Chapel Hill, NC 27599-3300, USA*

<sup>c</sup>*Department of Geosciences, University of California, Irvine, CA 92717, USA*

(Received December 15, 1992; revision accepted August 23, 1993)

## ABSTRACT

Sugai, S.F., Alperin, M.J. and Reeburgh, W.S., 1994. Episodic deposition and  $^{137}\text{Cs}$  immobility in Skan Bay sediments: A ten-year  $^{210}\text{Pb}$  and  $^{137}\text{Cs}$  time series. In: M.I. Scranton (Editor), Variability in Anoxic Systems. *Mar. Geol.*, 116: 351–372.

A geochronology time series provides a powerful tool for elucidating sedimentary processes such as episodic deposition and diffusive mobility of particle-reactive constituents. Depth distributions of  $^{210}\text{Pb}$  and  $^{137}\text{Cs}$  from Skan Bay, Alaska were determined for sediment cores collected in 1980, 1984, 1987, and 1990. Sediment X-radiographs reveal distinct layers indicating that sediments were not continuously mixed by bioturbation. However, the geochronology time series is inconsistent with an undisturbed, steady-state sediment column. Profiles from 1980, 1984, and 1990 reveal subsurface regions in which  $^{210}\text{Pb}$  activity is relatively constant. In addition, the depth of the primary  $^{137}\text{Cs}$  maximum (reflecting the 1963 peak in atmospheric bomb testing) does not increase in a regular fashion between 1980 and 1990. The  $^{210}\text{Pb}$  and  $^{137}\text{Cs}$  geochronologies can be reconciled by removing the effects of an instantaneous depositional event. The average  $^{210}\text{Pb}$  sedimentation rate (corrected for episodic deposition) in cores that were collected over a ten year period ( $0.241 \pm 0.006 \text{ g cm}^{-2} \text{ yr}^{-1}$ ) is in excellent agreement with the average  $^{137}\text{Cs}$  sedimentation rate ( $0.258 \pm 0.008 \text{ g cm}^{-2} \text{ yr}^{-1}$ ) calculated from three stratigraphic markers [peak fallout (1963), first appearance in the sediment record (1952), and the Chernobyl accident (1986)]. The mobility of bomb-derived  $^{137}\text{Cs}$  under in situ conditions was evaluated by a time-dependent numerical model applied to the  $^{137}\text{Cs}$  time series. The model indicates that bomb-derived cesium is immobile in Skan Bay sediments with a solid–liquid distribution coefficient ( $K_d$ ) of  $\geq 10^5 (\text{ml g}^{-1})$ .

## Introduction

Stratigraphic signals preserved in sediment records provide a means of detecting environmental changes that occurred during the past. A meaningful interpretation of sediment records requires that the relationship between depth and age be accurately known. The most widely used methods for establishing sediment geochronologies are based on tracers such as  $^{210}\text{Pb}$  and  $^{137}\text{Cs}$ . Reliable sediment accumulation rates can be determined from depth profiles of these tracers provided that deposition rates have remained relatively constant over time.

However, in coastal environments, steady-state deposition is often interrupted by episodic events. Although the frequency of such events may be

low, the quantity of material deposited may account for a significant portion of the sediment column. Profiles of  $^{210}\text{Pb}$  and  $^{137}\text{Cs}$  from a single time point often cannot differentiate episodic deposition from other sediment disturbances such as resuspension and bioturbation. By combining tracers with different input functions and a time series approach, an unambiguous geochronology is possible for a perturbed sediment column.

An added benefit of a  $^{137}\text{Cs}$  time series is that it provides a record of post-depositional mobility under in situ conditions. Large quantities of  $^{137}\text{Cs}$  were introduced to the marine environment by atmospheric nuclear bomb tests and by planned and accidental discharges from nuclear reactor facilities. Interest in understanding the mobility of this radionuclide in sediments stems from its preva-

lence in radioactive wastes, its widespread use as a geochronometric tracer, and its affinity for biological systems, functioning as a metabolic analog of potassium.

In this study,  $^{210}\text{Pb}$  and  $^{137}\text{Cs}$  profiles in anoxic sediments from Skan Bay, Alaska were measured at four different times between 1980 and 1990. The two tracers yield the same sedimentation rate provided that profiles are corrected for an episodic depositional event. A time-dependent model applied to "episodically"-corrected  $^{137}\text{Cs}$  profiles suggests that bomb-derived  $^{137}\text{Cs}$  is immobile in Skan Bay sediments. The  $^{137}\text{Cs}$  solid–liquid distribution coefficient predicted by the model is much greater than most values reported in the literature for marine and lacustrine sediments.

### Study site

Skan Bay is a two-armed, pristine embayment on the northwest side of Unalaska Island in the Aleutian chain (Fig. 1a). The southwestern arm ( $53^{\circ}37'\text{N}$ ,  $167^{\circ}03'\text{W}$ ) is 1.2 km at its widest point and has a broad sill reaching 10 m below the surface of the inlet (Fig. 1b). The basin of the southwestern arm has steep walls and functions as a sediment trap collecting water column particulates and debris from terrestrial run-off.

The broad, shallow sill prevents horizontal advection of oxygen-rich Bering Sea water into the basin. During the summer months, stable temperature and salinity gradients are established in the upper 30 m, effectively isolating deeper water. Because of its proximity to shore and funnel-like shape, the deep basin receives a relatively high flux of organic material. This high flux of organic matter, coupled with restricted circulation, results in seasonal depletion of oxygen within the water column. During the fall, the oxygen concentration at depths greater than 50 m drops to  $< 1 \text{ ml l}^{-1}$ . Skan Bay bottom waters are relatively isothermal with winter and summer temperatures varying between  $1^{\circ}$  and  $4^{\circ}\text{C}$  (Alperin, 1988).

Sediment cores were collected in the deepest portion of the basin at 65 m depth. The flocculent surface sediment has a high water content ( $> 98\%$ ) and contains 27% organic matter on a dry weight basis (Alperin et al., 1992). The sediment is black

from the surface to 40 cm ( $\sim 8.5 \text{ g cm}^{-2}$ ), becoming dark grey below that depth.

### Methods

#### *Sediment sampling and processing*

Sediment samples were collected using a box corer (Ocean Instruments, Inc.) capable of sampling a  $30 \times 30 \text{ cm}$  sediment area. The ship continuously rotated on its anchor chain but care was taken to sample when the ship was at approximately the same point of anchor swing. After core retrieval, water overlying the sediment was siphoned until 5 cm of bottom water remained. Up to 9 subcores could be taken from a box core by gently inserting clear plastic core liners (6.6 cm in diameter) into the sediment. This sub-sectioning of the box core resulted in shortening of the subcores by roughly 2 to 3 cm from that in the box corer, but all profiles are based upon a cumulative mass depth scale to remove effects of core compression during subsampling. Subcores were sectioned shortly after collection into 1 to 3 cm intervals and stored frozen in Whirlpaks™ (1980), lacquer-coated steel cans (1984), or ziplok bags (1987, 1990). Sediment collection dates, sampling intervals, and subcore descriptions are given in Table 1.

#### *Porosity*

Porosity was calculated from solid matter density ( $\rho_{\text{sm}}$ ), pore water density ( $\rho_{\text{pw}}$ ), and sediment water content ( $WC$ ). Solid matter density was measured by Quantichrome Corp. on two dried, finely ground sediment samples [from depths of 3 to 6 cm ( $2.33 \text{ g ml}^{-1}$ ) and 27 to 30 cm ( $2.34 \text{ g ml}^{-1}$ )] using a gas displacement technique. The densities were corrected for the salt contribution assuming the salt's density to be the same as NaCl. Pore water density was assumed to equal bottom water density ( $1.026 \text{ g ml}^{-1}$ ) which was calculated from temperature and salinity data. Water content, defined as the ratio of pore water mass to whole sediment mass, was measured by drying a known mass of whole sediment to constant weight. The

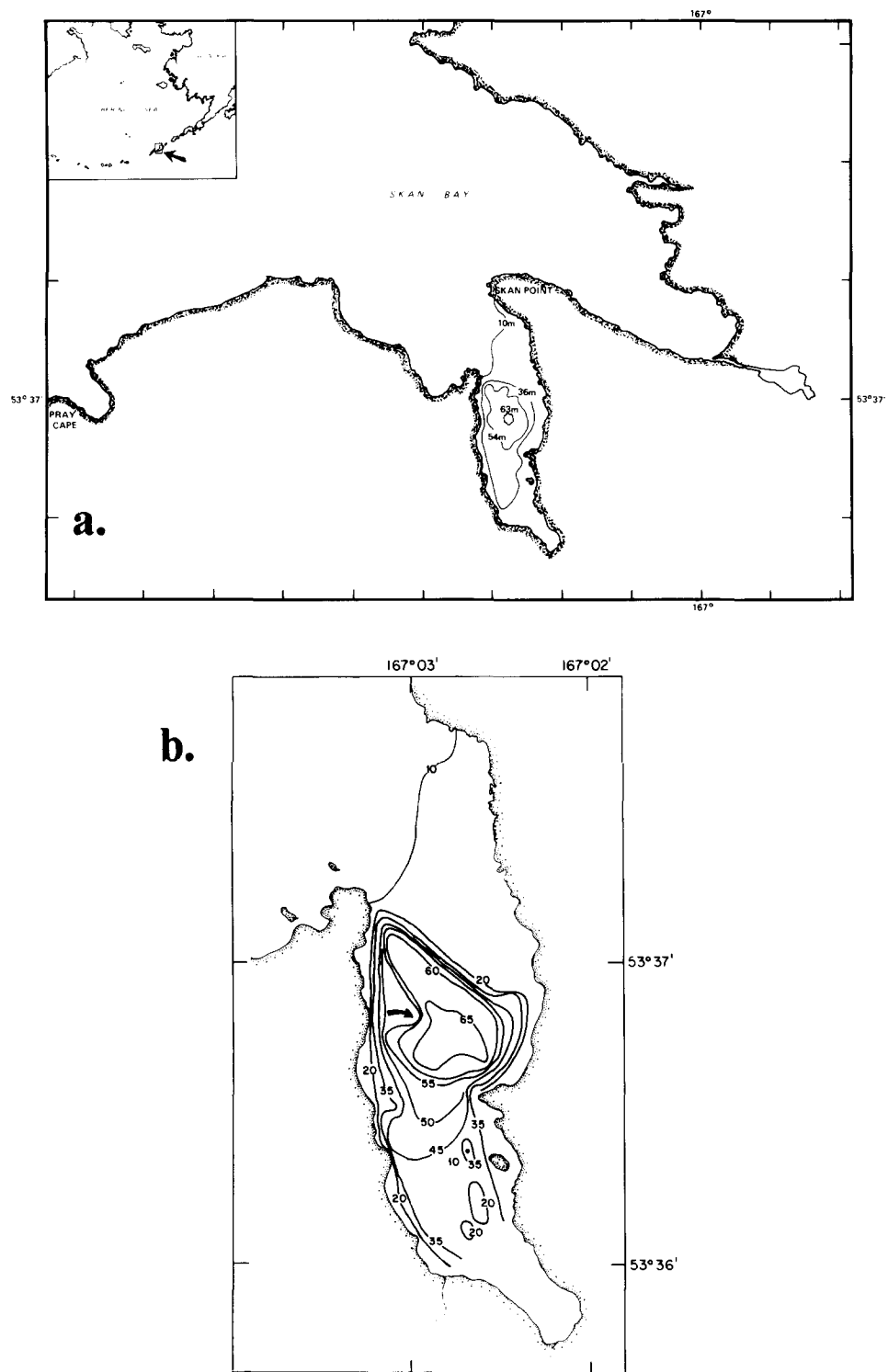


Fig. 1. (a) Location of Skan Bay, Alaska. The arrow on the inset map of Alaska points to Unalaska Island. (b) The southwestern arm of Skan Bay, Alaska. Sediment cores were collected within the 65 m isopleth. The arrow marks a possible origin of episodically deposited material.

TABLE 1

Sampling dates, subcore descriptions, and analyses

Subcore	Collection date	Approximate subcore length (cm)	Sampling interval (cm)	Analyses <sup>1</sup>
80WP	Sept. 1980 <sup>2</sup>	30	1	<sup>137</sup> Cs, <sup>210</sup> Pb-AD, porosity
80XR	16 Sept. 1980	40	3	X-radiography
84B <sup>3</sup>	27 Sept. 1984	40	3	<sup>137</sup> Cs
84C <sup>3</sup>	27 Sept. 1984	40	3	<sup>210</sup> Pb-AD
84D <sup>3</sup>	27 Sept. 1984	40	3	<sup>137</sup> Cs, <sup>210</sup> Pb-G, <sup>210</sup> Pb-AD, <sup>210</sup> Pb-AC, porosity
84G <sup>3</sup>	27 Sept. 1984	40	3	<sup>137</sup> Cs, <sup>210</sup> Pb-G
87A	7 Oct. 1987	40	2	<sup>137</sup> Cs, <sup>210</sup> Pb-G, porosity
90Z	13 July 1990	50	2	<sup>137</sup> Cs, <sup>210</sup> Pb-G, porosity

<sup>1</sup>G = gamma spectroscopy; AC = alpha spectroscopy, concentrated acid digestion; AD = alpha spectroscopy, dilute acid digestion. <sup>2</sup>Exact collection date is not known. <sup>3</sup>Subcores 84B, 84C, 84D are from the same box core; subcore 84G is from a different box core.

water content was calculated as:

$$WC = \frac{\text{mass whole sed.} - \text{mass dry sed.}}{\text{mass whole sediment}} \times \frac{\rho_{pw}}{\rho_{water}}$$

where  $\rho_{water}$  is the density of air-saturated water at 25°C. Porosity ( $\phi$ ) was calculated as:

$$\phi = \frac{WC\rho_{sm}}{WC\rho_{sm} + (1-WC)\rho_{pw}}$$

#### X-radiography

Subcores for X-radiography were taken by gently inserting a rectangular (18 × 2.5 × 60 cm) Plexiglass container into a sediment box core. The overlying water was siphoned and the subcore capped and stored upright at room temperature for several months. The seal on the container's bottom was imperfect allowing pore water to drain from the sediment. The loss of pore water allowed the sediments to consolidate for easy manipulation but resulted in compression of the depth scale. The subcores were X-rayed by a local veterinarian.

#### <sup>210</sup>Pb activity

Two methods were used to measure sediment <sup>210</sup>Pb activities: (1) alpha spectroscopy of <sup>210</sup>Po,

the short-lived daughter of <sup>210</sup>Pb, and (2) direct gamma spectroscopy. The analytical technique used for each subcore is given in Table 1.

Details of the <sup>210</sup>Po method are provided in Kipphut (1978). Briefly, a 2- to 3-g aliquot of dried, ground sediment was spiked with <sup>208</sup>Po (chemical yield tracer) and digested with boiling 2 N HCl for 6 h. Following digestion, the Po was electroplated onto silver discs in 1.2 N HCl at 80°C for 2 h. The discs were rinsed with distilled water, dried, and alpha-counted using Si surface-barrier detectors and alpha pulse-height analysis spectroscopy. The <sup>210</sup>Pb analyses were begun at least 15 months after sediment collection to assure secular equilibrium between <sup>210</sup>Pb ( $\tau_{1/2} = 22.2$  yr) and <sup>210</sup>Po ( $\tau_{1/2} = 0.378$  yr). Supported <sup>210</sup>Pb was estimated by averaging values determined by gamma spectroscopy of <sup>214</sup>Pb and <sup>214</sup>Bi on alternate subcores (described below). Excess <sup>210</sup>Pb was calculated by subtracting the supported from the total activity as described below in the section "Comparison of gamma and alpha spectroscopy" under "Results".

Subcore 84D was subjected to the concentrated acid digestion technique of Sugai (1990) in order to check for incomplete <sup>210</sup>Po extraction. The sediment was digested twice with boiling concentrated HNO<sub>3</sub> and HCl and the leachate was converted to chlorides by repeatedly adding HCl and evaporating to dryness. The residue was dissolved

in  $\sim 250$  ml of 0.3 N HCl and ascorbic acid was added to complex dissolved Fe. The Po was electroplated for 12 h onto 2.2 cm silver discs which had one side coated with an insulating varnish.

$^{210}\text{Pb}$  was also determined by direct gamma spectroscopy by quantifying the 46.5 keV peak using a Ge(Li) detector optimized for detection of low energy gamma photons. Aluminum cans were filled with 5- to 30-g dried, ground sediment and compressed with a stainless steel piston to a constant density. The cans were sealed and allowed to sit at least two weeks to assure secular equilibrium with respect to  $^{222}\text{Rn}$ . The detector was calibrated using synthetic standards made by diluting Standard Pitchblende Ore (US EPA, Las Vegas) with 99.5%  $\text{SiO}_2$  to produce a range of sample geometries.  $^{210}\text{Pb}$  activities were corrected for self-attenuation following the procedure of Cutshall et al. (1983). Background corrections for  $^{210}\text{Pb}$  were determined by counting empty aluminum cans. Supported  $^{210}\text{Pb}$  was determined by averaging  $^{214}\text{Pb}$  (295 keV),  $^{214}\text{Pb}$  (352 keV), and  $^{214}\text{Bi}$  (609 keV) peaks.

#### $^{137}\text{Cs}$ activity

$^{137}\text{Cs}$  activities were quantified by gamma spectroscopy (662 keV) using a Ge(Li) detector. Dried and ground sediment samples (5- to 30-g) were counted in either sealed aluminum cans or plastic petri dishes. The detector was calibrated with NBS SRM 4350B (Columbia River sediment) or known quantities of  $^{137}\text{Cs}$  diluted in 0.1 N HCl. Standards were prepared having a range of geometries that matched the sediment samples.

All sediment  $^{210}\text{Pb}$  and  $^{137}\text{Cs}$  data were corrected for the contribution of sea salt to sediment mass and decay-corrected to the time of core collection. The error estimate for each radioisotope analysis ( $\pm 1 \sigma$ ) was calculated by propagation of errors associated with sample and background counting rates.

#### Ammonium concentration

Interstitial ammonium was measured colorimetrically (Solorzano, 1969). Pore water was collected

by pressure filtration (1980, 1984, and 1990) or centrifugation (1987).

## Results

All sediment profiles are reported using the cumulative mass ( $\text{g cm}^{-2}$ ) depth scale to eliminate the effect of porosity changes with depth.

#### Porosity profiles

Sediment porosity was very high ( $> 0.97$ ) near the sediment–water interface (Fig. 2). Porosity generally decreased with depth, with most of the change occurring in the upper  $2 \text{ g cm}^{-2}$  ( $\sim 10 \text{ cm}$ ). Below this depth, porosities for six subcores collected between 1980 and 1990 fell within a relatively narrow range ( $0.88 \pm 0.02$ ,  $n = 66$ ).

#### X-radiography

Physical laminae visible in the X-radiograph indicate that sediments were not mixed by biotur-

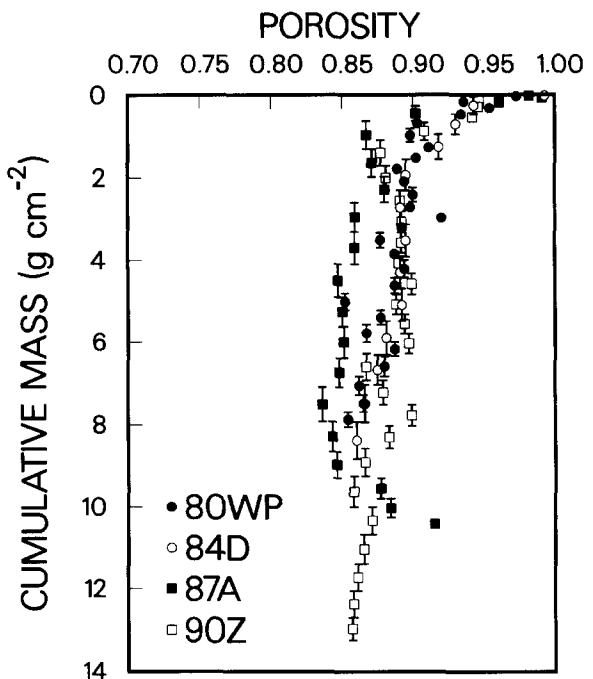


Fig. 2. Porosity versus cumulative mass for sediment cores collected in 1980, 1984, 1987 and 1990. The vertical bars represent the sample depth intervals; absence of a bar indicates that the interval is smaller than the symbol size.

bation (Fig. 3). The absence of burrows or tubes extending to the surface suggests that bioirrigation and methane ebullition were not active. Ten X-radiographs were taken and all showed similar light and dark striations at approximately regular intervals.

The X-radiograph is a positive image with light and dark regions corresponding to X-ray transparent and X-ray opaque sediment, respectively. The sediment appeared uniformly black to the naked-eye; the laminations were visible only by

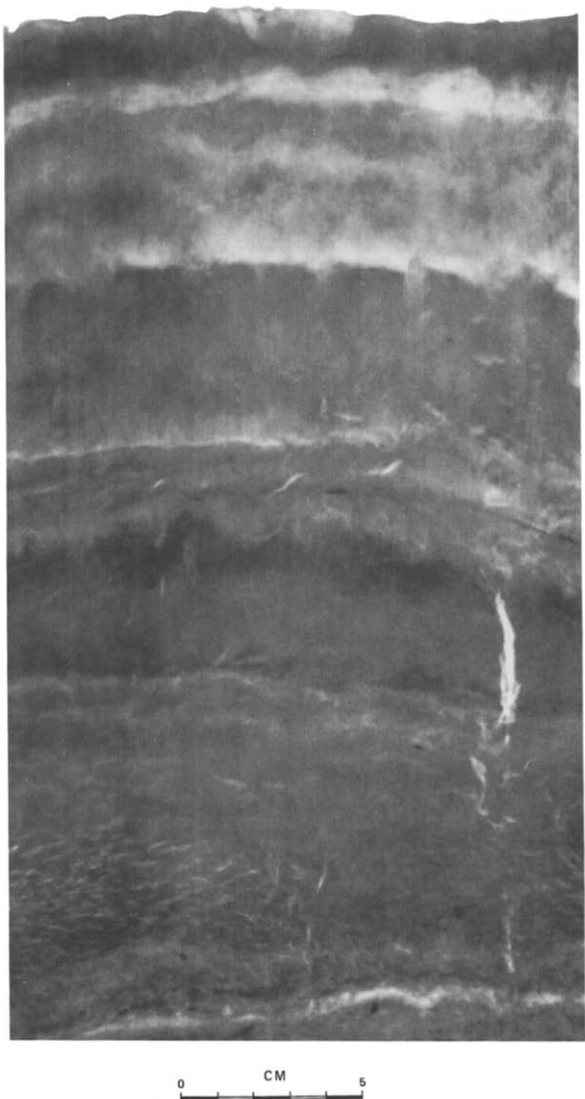


Fig. 3. Representative X-radiograph of sediment collected in 1980. The depth scale is compressed due to sediment desiccation.

X-radiography. The white vertical crescent in the lower right is a split in the sediment caused by desiccation. The slits that become prominent below 25 cm were created by methane bubbles that formed when the sediment decompressed after core retrieval. The small black circular objects scattered throughout the X-radiograph are probably fragments of mollusc shells.

#### $^{210}\text{Pb}$ profiles

$^{210}\text{Pb}$  is derived from  $^{222}\text{Rn}$ , an inert gas that emanates from the earth's crust and spreads through the atmosphere by advection and turbulence. The  $^{222}\text{Rn}$  decays to  $^{210}\text{Pb}$  which is transferred to the earth's surface by rain, snow, and dry deposition. The  $^{210}\text{Pb}$  that is deposited in aquatic environments is rapidly scavenged and incorporated into the sediment column. The activity of sedimentary  $^{210}\text{Pb}$  will decrease exponentially with depth (in accordance with its 22.3 yr half-life) provided that (1) the  $^{210}\text{Pb}$  deposition rate has been constant, (2) the sediments have not been disturbed, and (3) sediment  $^{210}\text{Pb}$  is not mobile. If these conditions are realized, the natural logarithm ( $\ln$ ) of excess  $^{210}\text{Pb}$  activities in sediment cores will decrease linearly with cumulative mass and the steady-state sediment accumulation rate can be calculated from the slope of the  $\ln$  excess  $^{210}\text{Pb}$  versus cumulative mass profile.

#### *Comparison of gamma and alpha spectroscopy*

Total  $^{210}\text{Pb}$  activities determined by gamma spectroscopy were consistently 40% higher than those determined by alpha spectroscopy (Fig. 4). Periodic gamma analysis of calibration standards (US EPA Pitchblende Ore) yielded  $^{210}\text{Pb}$  activities that agreed with expected values within the counting error. This suggests that  $^{210}\text{Pb}$  values determined by alpha spectroscopy are underestimated. Because gamma analysis detects lattice bound  $^{210}\text{Pb}$  that may resist acid leaching, incomplete extraction is a possible source of negative error in  $^{210}\text{Pb}$  concentrations determined by alpha counting. However, Cutshall et al. (1983) report no systematic differences between  $^{210}\text{Pb}$  concentrations determined by gamma and alpha spectroscopy for sediment samples having  $^{210}\text{Pb}$

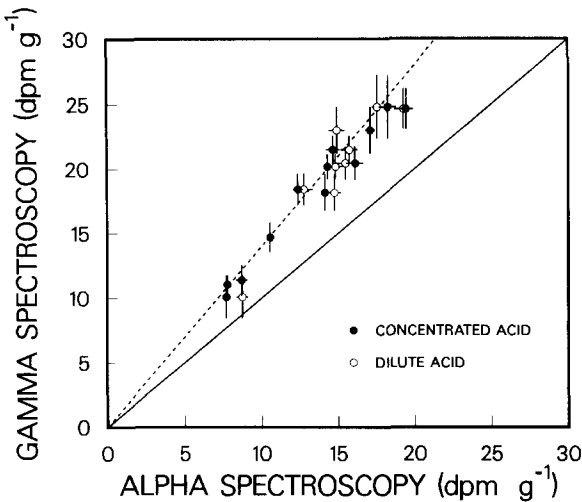


Fig. 4. Comparison of total  $^{210}\text{Pb}$  activities determined by gamma and alpha spectroscopy for sediment collected in 1984 (subcore 84D). Samples for alpha spectroscopy were extracted by concentrated and dilute acid digestion. The slope of the solid line is 1.0; the slope of the dashed line is 1.4. The error bars represent the statistical counting errors; absence of a bar indicates that the standard deviation is smaller than the symbol size.

concentrations comparable to those encountered in this study ( $\leq 22 \text{ dpm g}^{-1}$ ). Furthermore, agreement between  $^{210}\text{Pb}$  activities of replicate samples digested with concentrated or dilute acid (Fig. 4) suggests that incomplete extraction is not the cause of the systematic error. One possible source of error is the activity of the internal standard for alpha spectroscopy. Unfortunately, the  $^{208}\text{Po}$  solution no longer exists so this possibility cannot be tested. In order to allow a direct comparison between  $^{210}\text{Pb}$  profiles determined by alpha and gamma spectroscopy, activities determined by alpha counting have been multiplied by an empirical correction factor (1.4).

#### *Supported $^{210}\text{Pb}$*

Supported  $^{210}\text{Pb}$  activities are relatively constant with depth and show little interannual variability (Fig. 5). The average supported  $^{210}\text{Pb}$  value for four subcores collected between 1984 and 1990 is  $1.26 \pm 0.12 \text{ dpm g}^{-1}$  ( $n=68$ ). Supported values are much less than excess  $^{210}\text{Pb}$  (6 to 27 dpm  $\text{g}^{-1}$ , see below), indicating that  $^{210}\text{Pb}$  profiles are not affected by  $^{222}\text{Rn}$  diffusion (Imboden and Stiller,

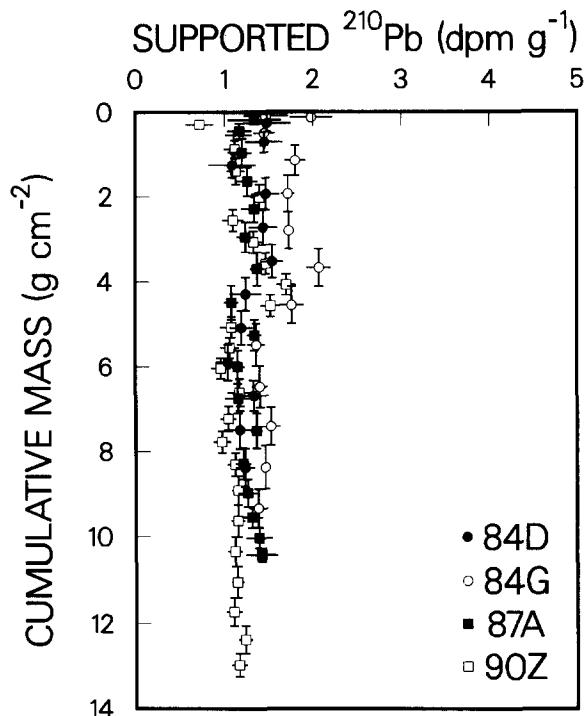


Fig. 5. Supported  $^{210}\text{Pb}$  versus cumulative mass for sediment cores collected in 1984, 1987 and 1990. The vertical bars represent the sample depth intervals; horizontal bars represent statistical counting errors. The absence of a bar indicates that sample interval or standard deviation are smaller than the symbol size.

1982). The absence of vertical and temporal gradients justifies using an average value to estimate supported  $^{210}\text{Pb}$  levels for samples analyzed by alpha spectroscopy.

#### *$^{210}\text{Pb}$ time series*

Values of ln excess  $^{210}\text{Pb}$  for sediment subcores collected between 1980 and 1990 generally decrease with cumulative mass (Fig. 6), but the profiles deviate in two ways from the linearity expected for steady-state deposition. First, profiles from 1980, 1984, and 1990 contain a subsurface region in which  $^{210}\text{Pb}$  activity remains relatively constant or increases slightly with depth. Second, maximum  $^{210}\text{Pb}$  activity in subcores collected in 1984, 1987, and 1990 occurs slightly below the sediment–water interface.

Several processes could be responsible for the subsurface discontinuity in the  $^{210}\text{Pb}$  profiles. The region could represent sediment homogenized by

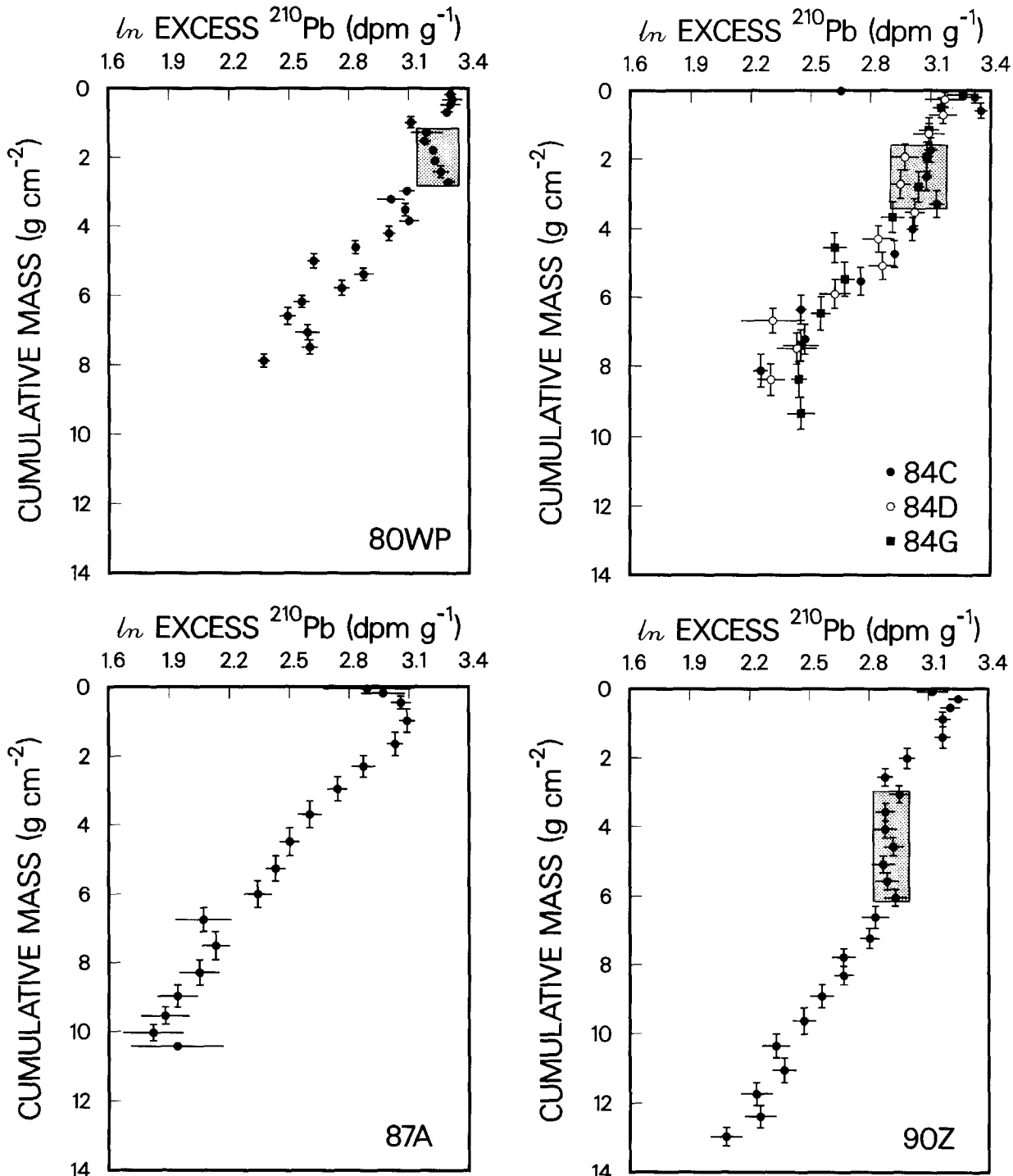


Fig. 6.  $\ln$  excess  $^{210}\text{Pb}$  versus cumulative mass for sediment collected in 1980, 1984, 1987 and 1990. The shaded boxes represent sediment attributed to an episodic event (the criteria used to define the zone of the instantaneous event are described in the text). Activities shown for subcore 84D were determined by gamma spectroscopy. The vertical bars represent the sample depth intervals; horizontal bars represent statistical counting errors. The absence of a bar indicates that sample interval or standard deviation are smaller than the symbol size.

a catastrophic storm event. However, mixing of Skan Bay sediment by wind-induced waves is unlikely since the broad 10 m sill (Fig. 1) and strong pycnocline restrict wave energy to the upper water column. Alternatively, the sediment could have been mixed by bioturbation. Laminations apparent in the X-radiograph (Fig. 3) do not preclude the possibility that sediments were intermittently inhabited by bioturbating organisms. The subsurface region of nearly constant  $^{210}\text{Pb}$  activity could also be accounted for by an event in which a large amount of sediment was deposited during a short time interval. This latter possibility is discussed in detail below.

The cause of maximum  $^{210}\text{Pb}$  concentrations slightly below the sediment–water interface is unknown. Low surface concentrations of  $^{210}\text{Pb}$  in non-bioturbated coastal sediments have been reported previously and attributed to Pb redistribution (Koide et al., 1973; Murray et al., 1978). However, sharp gradients in excess  $^{210}\text{Pb}$  at turbidite-laminae boundaries in Black Sea sediments argue against  $^{210}\text{Pb}$  mobilization in permanently anoxic sediments (Crusius and Anderson, 1991). Low  $^{210}\text{Pb}$  activities in surficial Skan Bay sediments may be related to the high porosity, organic-rich floc layer at the sediment–water interface.

#### *Sediment heterogeneity*

Replicate subcores collected in 1984 were analyzed for  $^{210}\text{Pb}$  to evaluate lateral sediment heterogeneity. Small-scale ( $\sim 10$  cm) patchiness was examined by comparing two subcores from the same box core (84C versus 84D) while large-scale ( $\sim 10$  m) variability was examined by comparing subcores from different box cores (84C and 84D versus 84G). The three  $^{210}\text{Pb}$  depth distributions show the same basic pattern (Fig. 6), suggesting that small-scale and large-scale variability in  $^{210}\text{Pb}$  activity are relatively minor. At most depth horizons,  $^{210}\text{Pb}$  activities in sediment from cores 84C, 84D, and 84G differ by less than 15%.

#### $^{137}\text{Cs}$ profiles

The introduction of large quantities of  $^{137}\text{Cs}$  to the marine environment began in 1952 with atmo-

spheric testing of thermonuclear explosives. Peak fallout occurred in 1963 and rapidly declined in subsequent years following ratification of the Nuclear Test Ban Treaty. The fallout  $^{137}\text{Cs}$  was scavenged by clay minerals in soil particles and transferred to marine or lacustrine sediments via erosion and runoff. The first appearance and maximum activity of bomb-derived  $^{137}\text{Cs}$  should occur at sediment depths corresponding to 1952 and 1963, respectively, provided that (1) the time between atmospheric deposition and incorporation into sediment is relatively short, (2) the sediments have not been disturbed, and (3) sediment  $^{137}\text{Cs}$  is not mobile. Radioactive fallout from the explosion and fire at the Chernobyl nuclear reactor in April 1986 resulted in additional  $^{137}\text{Cs}$  input to some regions of the northern hemisphere. Sites in Alaska detected  $^{137}\text{Cs}$  in atmospheric particles in early May 1986 (data cited in Davidson et al., 1987). The total quantity of  $^{137}\text{Cs}$  released during the Chernobyl accident (1 MCi) was small compared to that released by atmospheric testing of nuclear weapons (36 MCi) (Levi, 1986).

#### $^{137}\text{Cs}$ time series

The  $^{137}\text{Cs}$  profiles for all seven subcores exhibit a primary subsurface maximum reflecting the 1963 peak in atmospheric fallout (Fig. 7). However, the depth of the  $^{137}\text{Cs}$  peak does not increase with time in a regular fashion as would be expected for steady-state sediment deposition. The peak depth increased slightly between 1980 and 1984, decreased between 1984 and 1987, and increased substantially between 1987 and 1990. The erratic downward movement of the  $^{137}\text{Cs}$  maximum between 1980 and 1990 could reflect non-steady state sediment deposition or heterogeneous sedimentation throughout the deep basin. The sediment horizon marking the onset of thermonuclear tests in 1952 was reached only for the subcore collected in 1987.

The presence of Chernobyl-derived  $^{137}\text{Cs}$  in sediment cores collected after 1986 is equivocal. The activity of  $^{137}\text{Cs}$  in the uppermost sample in subcore 87A is slightly elevated relative to the next deepest sample. Likewise,  $^{137}\text{Cs}$  is slightly elevated at a depth of  $\sim 1 \text{ g cm}^{-2}$  in subcore 90Z. Unfortunately, high porosity in the surface sedi-

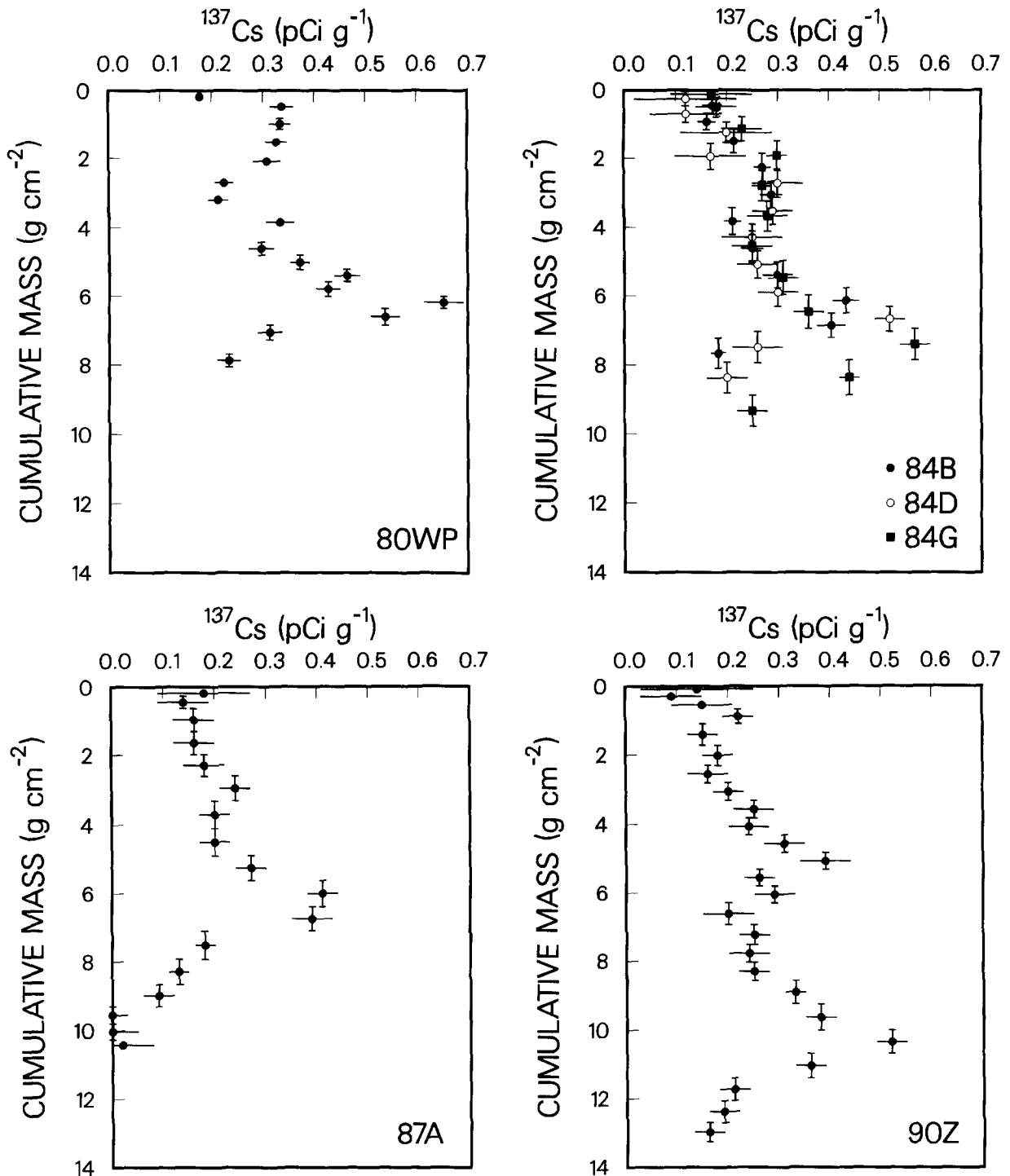


Fig. 7.  $^{137}\text{Cs}$  versus cumulative mass for sediment collected in 1980, 1984, 1987 and 1990. The vertical bars represent the sample depth intervals; horizontal bars represent statistical counting errors. The absence of a bar indicates that sample interval or standard deviation are smaller than the symbol size.

ment resulted in very small samples and poor counting statistics. Hence neither of the Chernobyl "peaks" exceed background by an amount greater than the counting error.  $^{134}\text{Cs}$  was also released during the Chernobyl fire but was not detected in any sediment samples. This is not surprising because the quantity released by the explosion was only half that of  $^{137}\text{Cs}$  (Devell et al., 1986) and the short half-life (2.06 yr) resulted in decay of more than three-quarters of the  $^{134}\text{Cs}$  prior to analysis.

#### *Sediment heterogeneity*

Replicate subcores collected in 1984 were analyzed for  $^{137}\text{Cs}$  to evaluate lateral sediment heterogeneity. Subcores 84B and 84D were taken from the same box core while 84G was from a different box core. Above the primary  $^{137}\text{Cs}$  peak ( $\leq 6 \text{ g cm}^{-2}$ ), activities for the three subcores agree within counting errors (Fig. 7). Lateral heterogeneity increases in the vicinity of the  $^{137}\text{Cs}$  maximum as expected for a region of strong vertical gradients. Maximum  $^{137}\text{Cs}$  activity for 84D is higher than 84B, probably because the latter peak is split between two adjacent depth intervals. The peak for 84G occurs about  $1 \text{ g cm}^{-2}$  below that for 84B and 84D, suggesting a moderate degree of heterogeneity in  $^{137}\text{Cs}$  activity.

#### *Ammonium profiles*

Pore-water ammonium concentrations increase from less than  $1 \text{ mM}$  near the sediment–water interface to more than  $3 \text{ mM}$  at depth (Fig. 8). At depths greater than  $4 \text{ g cm}^{-2}$  ( $\sim 20 \text{ cm}$ ), ammonium concentrations exceed  $2 \text{ mM}$ .

#### **Discussion**

##### *Episodic sediment deposition*

The Skan Bay  $^{210}\text{Pb}$  and  $^{137}\text{Cs}$  time series are inconsistent with a steady-state, undisturbed sediment column. The subsurface discontinuity in excess  $^{210}\text{Pb}$  (Fig. 6) suggests an instantaneous deposition event or an intermittent period of sediment mixing. The irregular downward progression of the  $^{137}\text{Cs}$  maximum (Fig. 7) suggests lateral

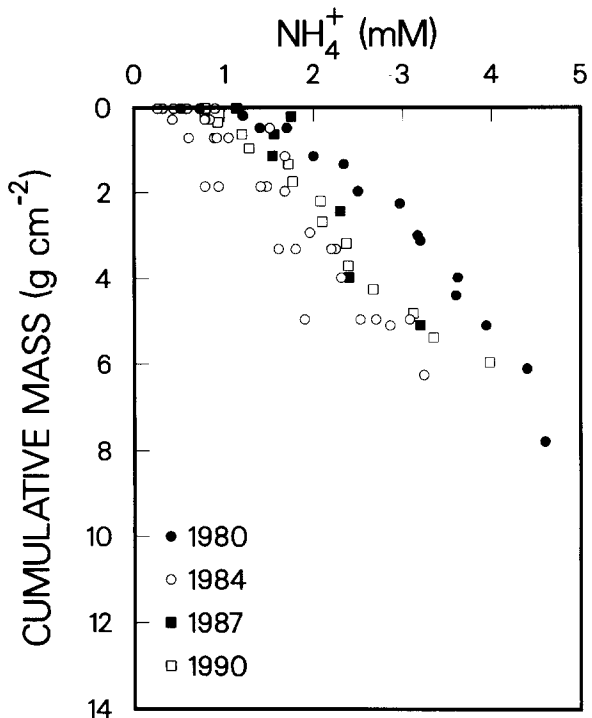


Fig. 8. Pore water ammonium versus cumulative mass for sediment pore waters collected in 1980, 1984, 1987 and 1990.

heterogeneity and/or non-steady state deposition. In this section, we demonstrate that  $^{210}\text{Pb}$  and  $^{137}\text{Cs}$  sedimentation rates agree if the profiles are corrected for the effect of an episodic depositional event.

The subsurface region of constant excess  $^{210}\text{Pb}$  serves to roughly define the zone containing episodically-derived sediment. For subcores collected in 1980, 1984, and 1990, the  $^{210}\text{Pb}$  discontinuity is centered about  $2.0$ ,  $2.5$ , and  $4.6 \text{ g cm}^{-2}$  below the sediment surface, respectively (Fig. 6). A zone of constant excess  $^{210}\text{Pb}$  is absent from the 87A profile, suggesting that this subcore was not influenced by episodic deposition.

The excess  $^{210}\text{Pb}$  profiles do not provide a basis for precisely locating the upper and lower boundaries of episodically deposited material. Since episodically-derived material is likely to contain recently deposited sediment, the zone of constant excess  $^{210}\text{Pb}$  could contain material that accumulated before and after the resuspension event. The  $^{137}\text{Cs}$  profiles provide an independent estimate of the vertical extent of the episodically-derived mate-

rial. This thickness is taken to be the cumulative mass required to bring  $^{137}\text{Cs}$  profiles from 1980 through 1990 into concordance. The  $^{137}\text{Cs}$  sedimentation rate for 87A ( $0.266 \text{ g cm}^{-2} \text{ yr}^{-1}$ ) was calculated assuming that sediment associated with the primary maximum was deposited in the year 1963. [The excess  $^{210}\text{Pb}$  profile for subcore 87A (Fig. 6) indicates that these sediments were not significantly affected by episodic deposition.] The thickness of the instantaneously deposited material for subcores collected in 1980, 1984, and 1990 (Table 2) was taken to be the difference between the expected depth of the 1963 horizon (calculated from the  $^{137}\text{Cs}$  sedimentation rate) and the actual depth of the  $^{137}\text{Cs}$  peak.

The shaded boxes in Fig. 6 illustrate the depth and thickness of the episodic event for each subcore. The magnitude varies between cores collected in different years, suggesting that instantaneously-derived sediment is not evenly distributed throughout the deep basin. This is not surprising since

regions closest to the origin of the episodic event are likely to receive a greater proportion of the deposition. Varying quantities of episodically-derived material in cores collected at different times is to be expected from random sampling of deep basin sediments.

Profiles of ln excess  $^{210}\text{Pb}$  (corrected for episodic deposition) versus cumulative mass are shown in Fig. 9. The plots are linear (average  $r^2 = 0.94$ ) and  $^{210}\text{Pb}$  sedimentation rates for cores collected over a 10 year period generally agree within 10% (Table 2). Likewise, excess  $^{210}\text{Pb}$  surface activities (calculated as the  $x$ -intercept of the least-squares line fitted to the ln excess  $^{210}\text{Pb}$  versus cumulative mass data) are comparable for all six subcores (Table 2). The linearity and consistency of the corrected  $^{210}\text{Pb}$  profiles suggest that sediment accumulation rates before and after the event were relatively constant.

Excess  $^{210}\text{Pb}$  activity in sediment comprising the episodic event decreased by 28% between 1980

TABLE 2

Episodically corrected  $^{210}\text{Pb}$  sedimentation rates

Subcore	"Event" thickness <sup>1</sup> ( $\text{g cm}^{-2}$ )	$^{210}\text{Pb}$ sedimentation rate <sup>2</sup> ( $\text{g cm}^{-2} \text{ yr}^{-1}$ )	Excess $^{210}\text{Pb}$ surface activity <sup>3</sup> (dpm $\text{g}^{-1}$ )	Excess $^{210}\text{Pb}$ in "event" <sup>4</sup> (dpm $\text{g}^{-1}$ )	Estimated "event" date <sup>5</sup>
80WP	1.7	$0.209 \pm 0.015$	$27.9 \pm 0.3$	$25.3 \pm 0.3$	1975
84C	1.0 <sup>6</sup>	$0.197 \pm 0.015$	$30.6 \pm 0.4$	$22.2 \pm 0.2$	1976
84D	1.1	$0.229 \pm 0.024$	$26.3 \pm 0.5$	$19.5 \pm 0.5$	1976
84G	1.8	$0.273 \pm 0.030$	$23.3 \pm 0.4$	$21.3 \pm 0.2$	1977
84 composite <sup>7</sup>	—	$0.230 \pm 0.015$	$26.3 \pm 0.3$	—	—
87A	0.0	$0.234 \pm 0.012$	$23.3 \pm 0.5$	—	—
90Z	3.2	$0.261 \pm 0.009$	$26.0 \pm 0.2$	$18.2 \pm 0.2$	1977
Weighted average <sup>8</sup>		$0.241 \pm 0.006$	$26.3 \pm 0.1$		

<sup>1</sup>Calculated as the cumulative mass required to bring  $^{137}\text{Cs}$  profiles into concordance (see text).

<sup>2</sup>Calculated as  $-\lambda/m$ , where  $\lambda$  is the  $^{210}\text{Pb}$  decay constant ( $0.0311 \text{ yr}^{-1}$ ) and  $m$  is the slope of the least-squares line fitted to the ln excess  $^{210}\text{Pb}$  vs. cumulative mass data. The uncertainty is calculated from the standard error of the slope. The surficial samples with low  $^{210}\text{Pb}$  activities were not included in the linear regression.

<sup>3</sup>Calculated as the  $x$ -intercept of the least-squares line fitted to the ln excess  $^{210}\text{Pb}$  versus cumulative mass data. The uncertainty is calculated from the standard error of the intercept. The surficial samples with low  $^{210}\text{Pb}$  activities were not included in the linear regression.

<sup>4</sup>Mean activity in sediment region attributed to an episodic event (see text).

<sup>5</sup>Calculated from cumulative mass at the top of the region attributed to an episodic "event", average  $^{210}\text{Pb}$  sedimentation rate, and date of core collection.

<sup>6</sup>There are no  $^{137}\text{Cs}$  data for 84C, so "event" thickness is taken as the average for subcores 84B ( $0.9 \text{ g cm}^{-2}$ ) and 84D.

<sup>7</sup>Sedimentation rate and surface activity are based on linear regression of combined 84C, 84D, and 84G data.

<sup>8</sup>Weighted averages are based on 80WP, 84 composite, 87A, and 90Z.

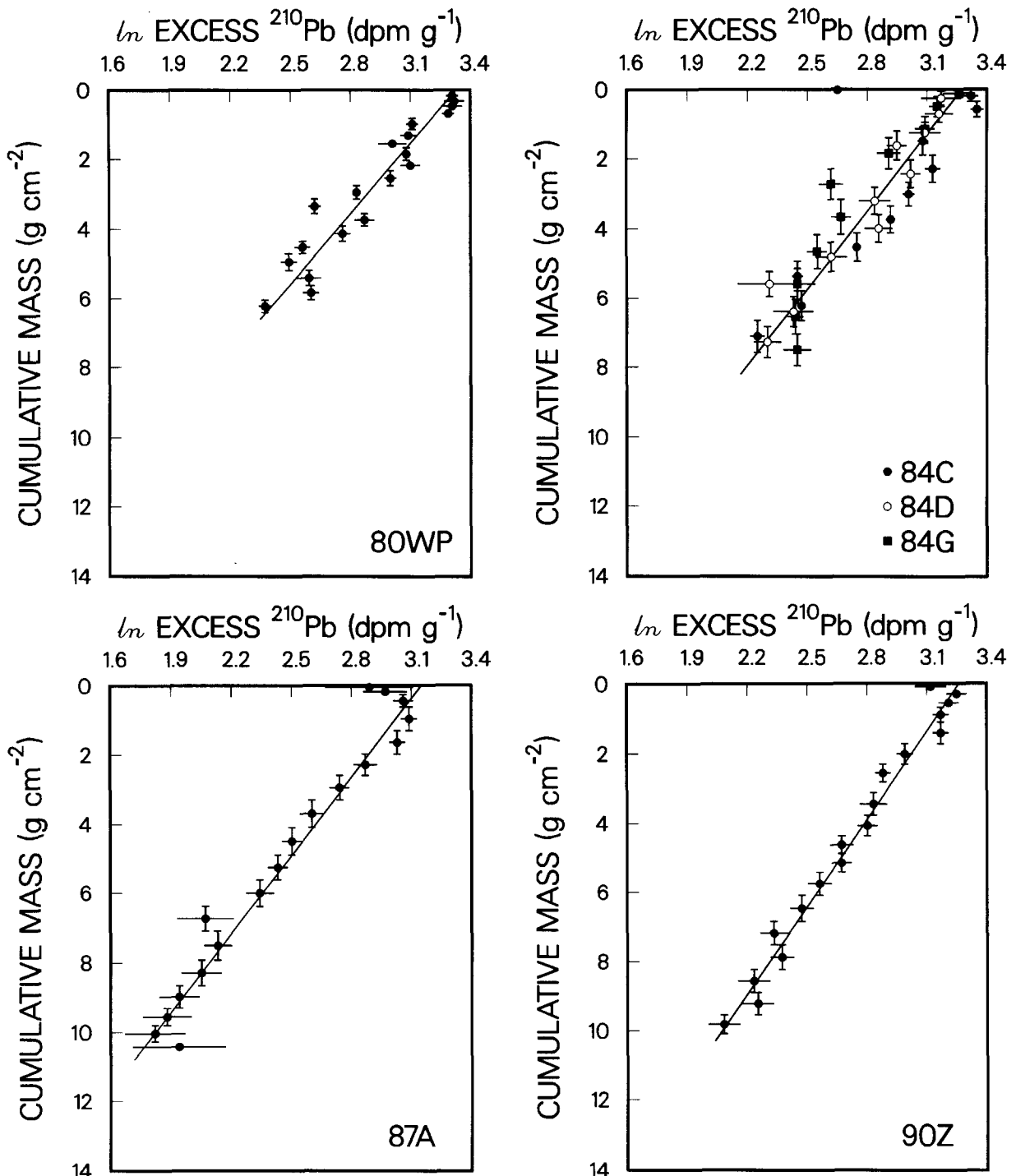


Fig. 9.  $\ln$  excess  $^{210}\text{Pb}$  versus cumulative mass (corrected for episodic deposition) for sediment collected in 1980, 1984, 1987, and 1990. The lines represent least-square fits to the data. The low  $^{210}\text{Pb}$  activities near the sediment–water interface were not included in the linear regression. The line shown in the 84C, 84D, and 84G panel represents a fit to the composite 1984 data set. The vertical bars represent the sample depth intervals; horizontal bars represent statistical counting errors. The absence of a bar indicates that sample interval or standard deviation are smaller than the symbol size.

and 1990 (Table 2). This compares favorably with the decrease expected from  $^{210}\text{Pb}$  decay (27%). The date of the event was estimated from the cumulative mass at the top of the region of relatively constant activity and the mean  $^{210}\text{Pb}$  sedimentation rate (Table 2). Although relatively coarse depth resolution limits the accuracy of the date estimate (i.e., each 2-cm sediment interval integrates  $\sim 2$  year accumulation), the data suggest that the resuspension event occurred sometime between 1976 and 1977 (Table 2). Decay correction of excess  $^{210}\text{Pb}$  in the episodic event for the time elapsed between deposition and core collection yields an average value of  $27.5 \pm 1.9$  dpm g $^{-1}$ , comparable to the average surface activity (Table 2). This suggests that the resuspended material was recently deposited surface sediment. The fan-like structure on the northwest side of the basin (Fig. 1b) represents a possible deposition site.

$^{137}\text{Cs}$  distributions corrected for episodic deposition are shown in Fig. 10. The “removal” of instantaneously-derived sediment results in profiles in which the depth of maximum  $^{137}\text{Cs}$  activity increases regularly with time. Sedimentation rates calculated from three  $^{137}\text{Cs}$  markers agree within the uncertainty associated with each (Table 3). Furthermore,  $^{210}\text{Pb}$  (Table 2) and  $^{137}\text{Cs}$  (Table 3) sedimentation rates corrected for episodic deposition are similar. This high level of internal consistency provides compelling evidence in support of a major episodic event.

Evidence of episodic deposition has been noted

for sediments from a wide variety of environments including lakes (e.g., Robbins, 1978), estuaries (e.g., Hirschberg and Schubel, 1979), coastal lagoons (e.g., Chanton et al., 1983), and fjords (e.g., Smith and Walton, 1980; Sugai, 1990; Paetzel and Schrader, 1992). For these environments, the deposition event is generally associated with a catastrophic storm or sudden perturbation to the watershed. In Skan Bay, the sediment resuspension may have been triggered by an earthquake. During the period between 1974 and 1979, at least five earthquakes with epicenters less than  $1.3^\circ$  latitude and  $3^\circ$  longitude from Skan Bay had magnitudes between 5 to 6 on the Richter scale (Brockman et al., 1988). The high frequency of earthquakes makes it impossible to link the Skan Bay instantaneous deposition to a particular tectonic event.

#### $^{137}\text{Cs}$ mobility

The degree of  $^{137}\text{Cs}$  mobility in lacustrine and marine sediments remains a matter of debate. Francis and Brinkley (1976) showed that sediment-bound  $^{137}\text{Cs}$  is preferentially sorbed onto micaeuous clay minerals such as illite. Because of its low charge density and thin hydration layer, the cesium ion can migrate into the internal structure of illite (Evans et al., 1983). Once inside the clay interlayer, the cesium loses its water of hydration allowing the illite to collapse and form a more stable structure (Sawhney, 1972). Studies of cesium sorption by illite suggest that frayed edges and interlayers retain cesium with a high degree of selectivity (Brouwer et al., 1983). These “super-selective” sites comprise only a small fraction of the clay’s total cation exchange capacity, but the solid–liquid distribution coefficient is so large that cesium sorbed at these sites is effectively immobilized (Cremers et al., 1988). Lominick and Tamura (1965) performed desorption experiments using illite-rich lake sediment contaminated by nuclear reactor discharge. They found that sediment  $^{137}\text{Cs}$  was not effectively extracted by solutions containing  $\text{KMnO}_4$ ,  $\text{NaOH}$ , 1 N  $\text{HNO}_3$ ,  $\text{NaCl}$ , or  $\text{CaCl}_2$ . Significant amounts of  $^{137}\text{Cs}$  were released only by extraction with 6 N  $\text{HNO}_3$ , which presumably destroyed the clay lattice structure.

In contrast, there is a growing body of evidence

TABLE 3

$^{137}\text{Cs}$  sedimentation rates corrected for episodic deposition

Method	$^{137}\text{Cs}$ sedimentation rate <sup>1</sup> (g cm $^{-2}$ yr $^{-1}$ )
Primary maximum in 87A corresponds to 1963	$0.266 \pm 0.015^2$
First appearance in 87A corresponds to 1952	$0.256 \pm 0.009$
Upper peak in 90Z corresponds to May 1986	$0.212 \pm 0.051$
Weighted average	$0.258 \pm 0.008$

<sup>1</sup>Error estimates are based on the size of the depth interval.

<sup>2</sup>The depth of maximum activity was taken as the midpoint between the two samples that comprise the peak.

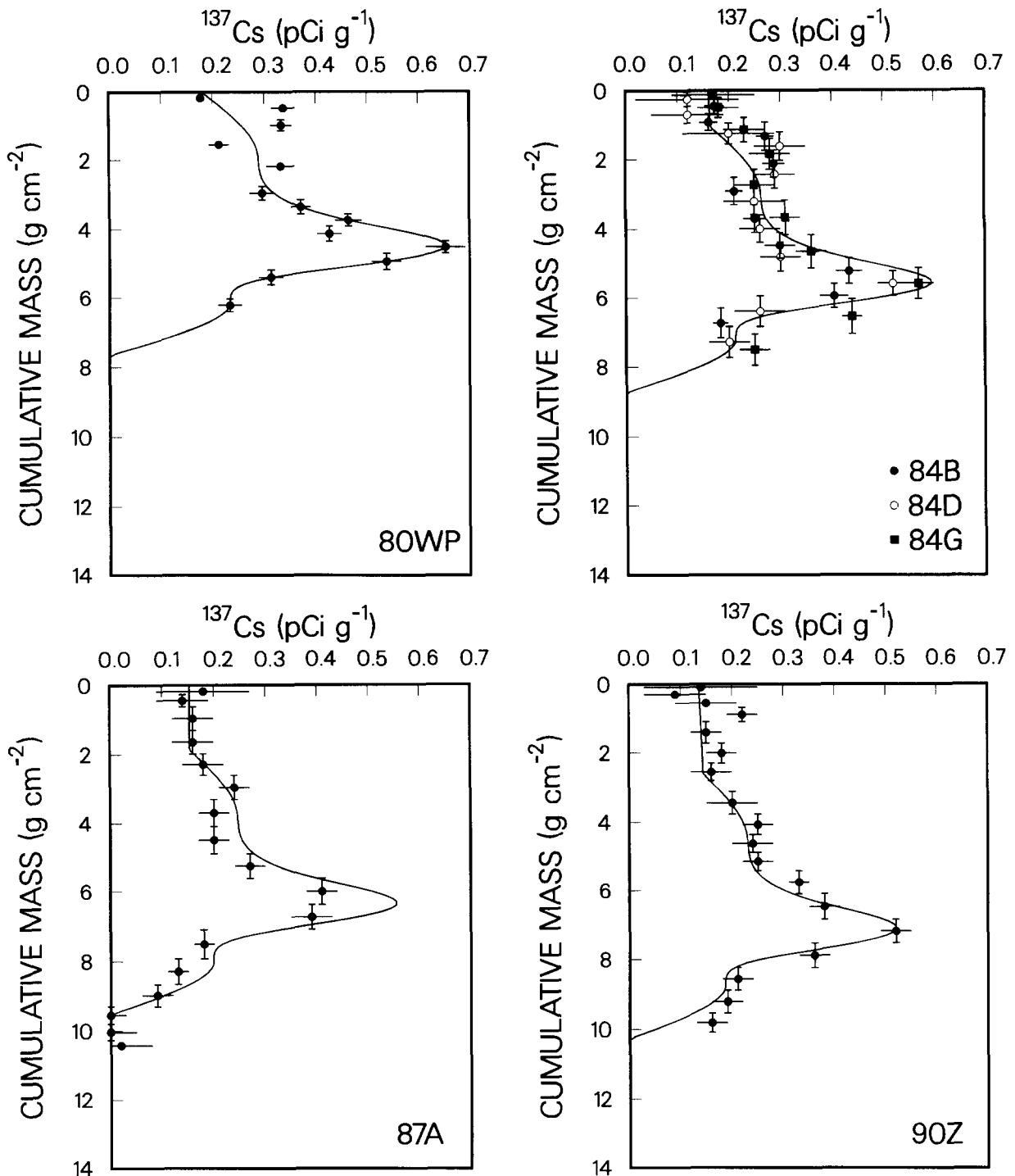


Fig. 10.  $^{137}\text{Cs}$  versus cumulative mass (corrected for episodic deposition) for sediment collected in 1980, 1984, 1987 and 1990. The curve in the 80WP panel represents the smoothed profile used to initialize the model. The curves shown in subsequent panels represent model-predicted profiles assuming no  $^{137}\text{Cs}$  mobility. The model used to generate the  $^{137}\text{Cs}$  profiles is described in the text. The vertical bars represent the sample depth intervals; horizontal bars represent statistical counting errors. The absence of a bar indicates that sample interval or standard deviation are smaller than the symbol size.

that supports post-depositional mobility of  $^{137}\text{Cs}$ . Elevated summertime activities in the water column of a pond containing sediment that had been contaminated by effluent from a faulty nuclear reactor suggest that anoxic conditions promote  $^{137}\text{Cs}$  mobility (Alberts et al., 1979). Laboratory desorption experiments using the same contaminated sediment suggest that  $^{137}\text{Cs}$  release is stimulated by ion-exchange with ammonium ion (Evans et al., 1983). Other studies using estuarine sediment contaminated by nuclear reactor discharge establish that  $^{137}\text{Cs}$  is desorbed when sediments are exposed to seawater (Patel et al., 1978; Stanners and Aston, 1981). Numerous studies in which uncontaminated sediments were spiked with  $^{137}\text{Cs}$  or  $^{134}\text{Cs}$  and allowed to equilibrate for several weeks to several months also demonstrate that radiocesium is readily desorbed from sediment particles (e.g., Santschi et al., 1983; Torgersen and Longmore, 1984; Comans et al., 1991).  $^{137}\text{Cs}$  mobility in lacustrine and marine sediments is also supported by pore water measurements which reveal small but significant quantities of dissolved  $^{137}\text{Cs}$  (Sholkovitz et al., 1983; Sholkovitz and Mann, 1984; Comans et al., 1989). In addition, sediment depth distributions of  $^{137}\text{Cs}$ ,  $^{239,240}\text{Pu}$ , and  $^{210}\text{Pb}$  provide evidence of  $^{137}\text{Cs}$  mobility. The  $^{239,240}\text{Pu}/^{137}\text{Cs}$  ratio has been observed to decrease with depth, suggesting preferential downward migration of  $^{137}\text{Cs}$  (Beasley et al., 1982; Sholkovitz and Mann, 1984). Likewise,  $^{137}\text{Cs}$  penetration to depths much greater than expected from  $^{210}\text{Pb}$  dating (e.g., Torgersen and Longmore, 1984) is consistent with post-depositional migration of  $^{137}\text{Cs}$ .

The Skan Bay  $^{137}\text{Cs}$  time series (Fig. 10) provides an opportunity to assess  $^{137}\text{Cs}$  mobility under in situ conditions. The profiles for sediment cores collected between 1980 and 1990 represent an empirical record of migration of bomb-derived  $^{137}\text{Cs}$  during a 10 year period. In the following section, diffusive redistribution of  $^{137}\text{Cs}$  in Skan Bay sediments is evaluated using a numerical model to simulate  $^{137}\text{Cs}$  profiles for various degrees of mobility.

Spatial and temporal changes in  $^{137}\text{Cs}$  activity resulting from sorption, diffusive migration, sediment accumulation, and radioactive decay are

described by the following equation (Lerman, 1977; Lynch and Officer, 1984):

$$\frac{\partial c}{\partial t} = \frac{D^*_s}{1 + K^*_d} \frac{\partial^2 c}{\partial x^2} - \omega \frac{\partial c}{\partial x} - \lambda c \quad (1)$$

where

$c = ^{137}\text{Cs}$  activity per unit mass of solid sediment ( $\text{pCi g}^{-1}$ );

$t = \text{time (year)}$ ;

$D^*_s = \text{sediment diffusion parameter}$  ( $\text{cm}^2 \text{ yr}^{-1}$ );

$K^*_d = \text{solid-liquid distribution coefficient}$ :

$$\left( \frac{\text{pCi}_{\text{sorbed}} \text{g}_{\text{solid}}^{-1}}{\text{pCi}_{\text{dissolved}} \text{g}_{\text{solid}}^{-1}} \right)$$

$x = \text{cumulative mass depth}$  ( $\text{g cm}^{-2}$ );

$\omega = \text{sediment accumulation rate}$  ( $0.266 \text{ g cm}^{-2} \text{ yr}^{-1}$ );

$\lambda = \text{radioactive decay constant for } ^{137}\text{Cs}$  ( $0.0230 \text{ yr}^{-1}$ ).

The sediment diffusion parameter ( $D^*_s$ ) is related to the sediment diffusion coefficient ( $D_s$ ,  $\text{cm}^2 \text{ s}^{-1}$ ) by the following equation (Lynch and Officer, 1984):

$$D^*_s = D_s [\rho_{\text{sm}} (1 - \phi)]^2$$

$D_s$  was calculated from the free-solution diffusion coefficient ( $1.11 \times 10^{-5} \text{ cm}^2 \text{ s}^{-1}$ ) by correcting for sediment tortuosity (Ullman and Aller, 1982) using the average porosity below 2  $\text{g cm}^{-2}$  ( $\phi = 0.88$ ). The free-solution diffusion coefficient for  $^{137}\text{Cs}$  (assumed to be the same as stable cesium) was taken from Li and Gregory (1974) and adjusted to in situ temperature ( $3^\circ\text{C}$ ) and salinity (32‰) according to the Stokes-Einstein equation (Lerman, 1979).

The solid-liquid distribution coefficient defined above ( $K^*_d$ ) is dimensionless. Most experimental studies, however, express distribution coefficients as  $\text{ml}_{\text{pore water}} \text{ g}_{\text{solid}}^{-1}$ . The more conventional definition of distribution coefficient ( $K_d$ ) is related to  $K^*_d$  by the following expression:

$$K_d \left( \frac{\text{pCi}_{\text{sorbed}} \text{g}_{\text{solid}}^{-1}}{\text{pCi}_{\text{dissolved}} \text{ml}_{\text{pore water}}^{-1}} \right) = K^*_d \frac{\phi}{(1 - \phi)\rho_{\text{sm}}}.$$

The sediment accumulation rate ( $\omega = 0.266 \text{ g cm}^{-2} \text{ yr}^{-1}$ ) used in the model is based on the depth of

the primary  $^{137}\text{Cs}$  maximum for subcore 87A (Table 3). Although this value is slightly higher than weighted average sedimentation rates (Tables 2 and 3), its use assures that the depth of maximum  $^{137}\text{Cs}$  activity in the model-predicted profiles will coincide with the data corrected for instantaneous deposition. By forcing the predicted and measured peaks to coincide, the effect of diffusive redistribution (reflected in changes in peak magnitude and shape) will be more apparent.

The assumptions implicit in Eq. 1 are:

(a) *The sediment accumulation rate corrected for episodic deposition is constant.* This assumption is supported by several lines of evidence: (i) *In excess*  $^{210}\text{Pb}$  profiles corrected for instantaneous deposition are linear (Fig. 9), (ii) corrected  $^{210}\text{Pb}$  accumulation rates and surface activities for cores collected in 1980, 1984, 1987 and 1990 are consistent (Table 2), and (iii) sedimentation rates (corrected for instantaneous deposition) calculated by two geochronometers with distinct input functions ( $^{210}\text{Pb}$  and  $^{137}\text{Cs}$ ) are in good agreement (cf. Tables 2 and 3).

(b) *Sediments are not bioturbated.* The distinct layers and absence of burrows or tubes in the sediment X-radiograph (Fig. 3) support the assumption that surface sediments were not mixed by benthic organisms. In general, benthic organisms of any sort are rare in the deep basin of Skan Bay. We observed several individuals of *Nephthys cornuta cornuta* in the upper cm of one core collected in 1987, and a single ciliate worm (unidentified) in a core collected in 1992 from the shallow region indicated by the arrow in Fig. 1b. However, these are isolated incidents among the hundreds of cores collected over 12 years.

(c) *Porosity is constant with respect to time and depth.* The assumption of steady-state porosity is supported by profiles for cores collected between 1980 and 1990 (Fig. 2). The assumption of constant porosity with depth is justified because the model focuses on the primary  $^{137}\text{Cs}$  peak which is located below the region exhibiting a porosity gradient (cf. Figs. 2 and 7).

(d) *Horizontal gradients in  $^{137}\text{Cs}$  activity are small relative to vertical gradients.* The replicate subcores collected in 1984 (Fig. 7) illustrate that

moderate horizontal gradients are much smaller than vertical gradients.

(e)  *$^{137}\text{Cs}$  sorption follows a linear isotherm with a constant solid-liquid distribution coefficient.* Non-linear isotherms occur when an ion's concentration becomes comparable to the number of available exchange sites. For the case of cesium in marine sediments, simple linear sorption is expected because cesium is present at trace concentrations and sediments contain a large number of clay particles. Likewise,  $K_d$  values for  $^{137}\text{Cs}$  are thought to be relatively constant for a particular marine sediment because the concentration of ions competing for exchange sites is not significantly changed by cesium sorption (Duursma and Bewers, 1986).

The model was initialized using  $^{137}\text{Cs}$  data for sediment collected in 1980. The 80WP profile (corrected for episodic deposition) was smoothed to filter out scatter in the uppermost portion of the sediment column (Fig. 10). Note that the smoothing procedure does not bias  $^{137}\text{Cs}$  data in the vicinity of the primary maximum. Since subcore 80WP does not extend to the horizon marking the onset of thermonuclear testing, the profile was extrapolated to intersect the depth axis at  $7.7 \text{ g cm}^{-2}$  corresponding to the year 1952 (assuming  $\omega = 0.266 \text{ g cm}^{-2} \text{ yr}^{-1}$ ). The  $^{137}\text{Cs}$  activity at the upper boundary ( $x = 0 \text{ g cm}^{-2}$ ) was initially set to  $0.18 \text{ pCi g}^{-1}$  and allowed to decrease with time as expected for radioactive decay ( $\tau_{1/2} = 30.1 \text{ yr}$ ). The  $^{137}\text{Cs}$  activity at the lower boundary ( $x = 14 \text{ g cm}^{-2}$ ) was fixed at  $0 \text{ pCi g}^{-1}$ . Equation 1 was solved numerically using the method of lines with cubic Hermite polynomials (Sewell, 1982). Solutions were obtained at  $t = 4.0, 7.0$ , and  $9.8 \text{ years}$ , corresponding to the time that elapsed between collection of cores in 1980, 1984, 1987 and 1990 (Table 1).

The model was first run assuming no post-depositional mobility of  $^{137}\text{Cs}$  [i.e., the term  $D^*_{\text{s}}/(1+K^*_d)$  in Eq. 1 was set to 0]. The model predicts the depth of the primary  $^{137}\text{Cs}$  maximum for all profiles corrected for episodic deposition (Fig. 10). This is expected, of course, because the magnitude of the episodic correction was defined as the cumulative mass required to bring the  $^{137}\text{Cs}$  profiles into concordance. The significance of the

model lies in its ability to predict changes over time in the *magnitude* and *shape* of the  $^{137}\text{Cs}$  maximum. For subcores collected in 1984, the model-predicted profile is consistent with data from subcores 84D and 84G. Peak  $^{137}\text{Cs}$  activity for 84B is less than that predicted by the model, but the two-point maximum suggests that the highest activity sediment was split between two sample intervals. Likewise, the two-point maximum for 87A indicates that the primary  $^{137}\text{Cs}$  peak was not concentrated in a single sample. For subcore 90Z, the model does an excellent job of predicting both the magnitude and shape of the primary  $^{137}\text{Cs}$  peak. The model demonstrates that changes in episodically-corrected  $^{137}\text{Cs}$  profiles between 1980 and 1990 can be explained by sediment accumulation and radioactive decay without need to invoke diffusive mobility.

The model was next run assuming various degrees of post-depositional migration. Equation 1 was solved for  $K_d$  values ( $\text{ml}_{\text{pore water}} \text{ g}^{-1} \text{ solid}$ ) ranging from  $10^2$  to  $10^5$ . Since the 1990 profile provides the most sensitive indicator of  $^{137}\text{Cs}$  mobility (i.e., differences between profiles from 1980 and 1990 reflect an entire decade of diffusive redistribution), we will focus on model-predicted profiles for subcore 90Z (Fig. 11). The simulated  $^{137}\text{Cs}$  profile for  $K_d = 10^5$  provides an excellent fit to the data. Note that the model-predicted profile for  $K_d = 10^5$  is essentially identical to that predicted for the case of no diffusive mobility (Fig. 10). Simulated profiles for lower values of  $K_d$  are clearly inconsistent with measured  $^{137}\text{Cs}$  activities. The model predicts that the solid–liquid distribution coefficient for bomb-derived  $^{137}\text{Cs}$  in Skan Bay sediments is  $\geq 10^5 \text{ ml}_{\text{pore water}} \text{ g}^{-1} \text{ solid}$ .

Two approaches to measuring  $K_d$  values for cesium in marine and lacustrine sediments have seen widespread use. The first approach involves labelling the sediment–water system with trace quantities of dissolved radiocesium. The  $K_d$  for cesium adsorption is calculated from the fraction of tracer taken up by sediment particles. It is also possible to calculate a desorption  $K_d$  by monitoring radiocesium release after replacing the spiked aqueous phase with a tracer-free solution. Ideally, distribution coefficients determined by adsorption and desorption techniques would agree. In reality,

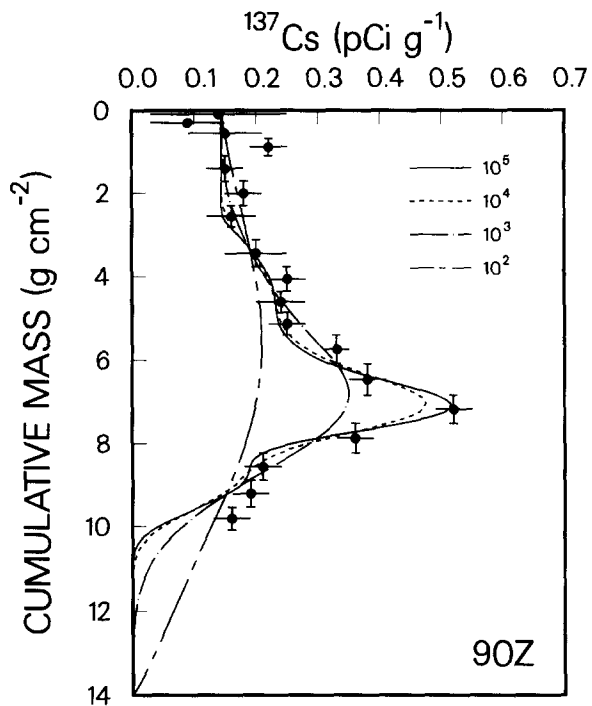


Fig. 11. Model predictions of  $^{137}\text{Cs}$  activity in 1990 for varying values of  $K_d$  ( $\text{ml}_{\text{pore water}} \text{ g}^{-1} \text{ solid}$ ). The  $^{137}\text{Cs}$  profile has been corrected for the effect of episodic deposition. The model used to generate the  $^{137}\text{Cs}$  profiles is described in the text. The vertical bars represent the sample depth intervals; horizontal bars represent statistical counting errors. The absence of a bar indicates that sample interval or standard deviation are smaller than the symbol size.

$K_d$  values determined by desorption are often much greater than those determined by adsorption, suggesting that neither technique reaches true equilibrium (Schell and Sibley, 1982).

The second approach to measuring  $K_d$  values involves determining the activity of  $^{137}\text{Cs}$  or  $^{134}\text{Cs}$  in sediment pore waters. This approach requires that relatively large quantities of filtered pore water be extracted by pressure filtration or centrifugation. The in situ solid–liquid distribution coefficient is directly calculated from measured solid phase and pore water radiocesium activities.

Literature values of cesium distribution coefficients for marine and lacustrine sediments are summarized in Table 4. Given the variety of experimental methods and sediment types involved in these studies, there is remarkably little variability in reported  $K_d$  values. Distribution coefficients determined by tracer experiments and pore-water

TABLE 4

Literature values of cesium solid-liquid distribution coefficient ( $K_d$ ) for marine and lacustrine sediments

Sediment source	$K_d^1$ (ml <sub>pore water</sub> g <sup>-1</sup> solid)	Technique	Reference
<i>(A) Tracer experiments</i>			
Atlantic, Pacific, and Indian Oceans; Baltic, North, Mediterranean, Black and Red Seas <sup>2</sup>	30–1300 (30) 80–740 (5)	Desorption Adsorption <sup>3</sup>	Duursma and Eisma (1973)
Ravenglass Estuary, UK	~300–500	Adsorption	Stanners and Aston (1981)
Lake Michigan, Hudson River, Clinch River, Cattaraugus Creek, Skagit Bay, Columbia River, Saanich Inlet, Lake Nitinat, Sinclair Inlet, Lake Washington (all USA)	1800–5600 (4) 50–1700 (17)	Desorption <sup>4</sup> Adsorption	Schell and Sibley (1982)
Narragansett Bay, USA	100–150	Adsorption	Santschi et al. (1983)
Narragansett Bay, USA; San Clemente Basin, USA; MANOP Station H (Eastern North Pacific)	140–400 (3) 140–400 (3)	Desorption Adsorption	Nyffeler et al. (1984)
Hidden Lake, Australia	140–190 25–40	Desorption Adsorption	Torgersen and Longmore (1984)
MANOP Stations M, L, H, C, S, R (Pacific Ocean)	~70–700 (6)	Adsorption	Buchholtz et al. (1986)
Study Site	$K_d$ (ml <sub>pore water</sub> g <sup>-1</sup> solid)	Reference	
<i>(B) Pore water measurements</i>			
Buzzards Bay, MA, USA	700		Sholkovitz et al. (1983)
Buzzards Bay, MA, USA	100–1000		Sholkovitz and Mann (1984)
Ketelmeer, Holland	50–1000		Comans et al. (1989)

<sup>1</sup>For studies that encompass multiple regions, the values in parentheses represent the number of different sites from which sediment was obtained. <sup>2</sup>Solid-liquid distribution coefficients (originally reported as ml<sub>pore water</sub> ml<sup>-1</sup> solid) were converted to ml<sub>pore water</sub> g<sup>-1</sup> solid assuming a solid matter density of 2.3 g ml<sup>-1</sup>. <sup>3</sup>One value that is clearly an outlier ( $K_d = 170,000$ ) has been omitted. <sup>4</sup> $K_d$  (desorption) values determined only for Lake Michigan and Hudson River sediment.

measurements are comparable, with most values falling between  $10^2$  and  $10^3$ .

The distribution coefficient consistent with the Skan Bay  $^{137}\text{Cs}$  time series ( $\geq 10^5$ , Fig. 11) is much larger than values reported in the literature ( $< 10^4$ , Table 4). There are a number of possible explanations for this apparent discrepancy. One possibility

is that the high  $K_d$  value for Skan Bay sediments is the result of an artifact associated with the model, the assumptions, or the numerical solution. However, the conclusion that bomb-derived  $^{137}\text{Cs}$  is not mobile (and hence has a large  $K_d$ ) is readily supported by a simple calculation. Fick's Second Law predicts that diffusive migration is most rapid

in the vicinity of minima and maxima. Therefore, the major effect of  $^{137}\text{Cs}$  mobility is to reduce the magnitude of the primary peak. The fact that peak  $^{137}\text{Cs}$  activity decreases by only 20% between 1980 and 1990 (i.e., 0.65 to 0.52 pCi g $^{-1}$ , Fig. 10), in agreement with that predicted by radioactive decay, is evidence against appreciable diffusive migration.

A second possible explanation for the discrepancy is that Skan Bay sediment has some property that renders it particularly effective for immobilizing bomb-derived  $^{137}\text{Cs}$ . Comans et al. (1989) report an inverse correlation between sediment  $K_d$  and ammonium concentration, suggesting that  $^{137}\text{Cs}$  is more strongly sorbed in ammonium-free sediments. However, Skan Bay pore waters are rich in ammonium with concentrations in excess of 2 mM at depths that coincide with the  $^{137}\text{Cs}$  peak (cf. Figs. 7 and 8). Clay mineral composition may also be an important factor in controlling sediment adsorption characteristics. Duursma and Eisma (1973) present evidence of a weak positive correlation between  $K_d$  and sediment illite content. The sediments surrounding the Aleutian Islands have illite contents of >20%, but the same is true for much the world's oceans (Lisitzin, 1972). The virtual absence of benthic organisms and the major contribution of kelp debris to the organic content of these sediments may have some unknown role in their ability to retain  $^{137}\text{Cs}$ .

A third explanation for the discrepancy is that different approaches to determining distribution coefficients are sensitive to disparate sorption processes. Cesium sorption by illite is thought to occur at a number of exchange sites (Sawhney, 1972), each having distinct specificity (Cremers et al., 1988) and sorption kinetics (Comans and Hockley, 1992). Since tracer experiments are conducted over time periods of days to weeks, distribution coefficients measured by this approach are relevant to ion exchange at the most accessible sites on the clay particles' exterior surface. The relatively low  $K_d$  values determined by tracer experiments ( $< 10^4$ ) reflect the fact that cesium sorbed at these surface sites is easily displaced by competing ions. In contrast, the distribution coefficient derived from this study (based on temporal changes in the primary  $^{137}\text{Cs}$  maximum) pertains to  $^{137}\text{Cs}$  that

has been in contact with clay minerals for several decades. The bomb-derived  $^{137}\text{Cs}$  has had sufficient time to diffuse to remote, highly selective interior sorption sites. The relatively high  $K_d$  value determined by this approach ( $\geq 10^5$ ) reflects the strong retention of cesium sorbed at interlayer sites. The precise meaning of distribution coefficients calculated from pore water radiocesium measurements is unclear.  $K_d$  values determined by this approach require the assumption that the dissolved phase (operationally defined by the nominal pore size of the filter) is free of colloidal cesium.

## Conclusions

(1) Steady-state sediment deposition in Skan Bay was punctuated by an episodic event that occurred in the mid-1970s. This episodic event appears to be the major departure from steady-state accumulation during the ~40 years represented by the sediment cores. The instantaneous event was composed of recently deposited surface sediment possibly derived from the steep walls surrounding the deep basin. Sedimentation rates (corrected for episodic deposition) determined by  $^{210}\text{Pb}$  and  $^{137}\text{Cs}$  yield an average deposition rate of  $0.250 \pm 0.005 \text{ g cm}^{-2} \text{ yr}^{-1}$ . This translates to a bulk sediment ( $\phi = 0.88$ ) accumulation rate of  $0.89 \pm 0.02 \text{ cm yr}^{-1}$ .

(2) Bomb-derived  $^{137}\text{Cs}$  appears to be immobile in Skan Bay sediments. A numerical model that considers only sediment accumulation and radioactive decay does an excellent job of predicting changes in the magnitude and shape of the  $^{137}\text{Cs}$  peak during the 10 year period bracketed by the time series. The model illustrates that the effect of diffusive migration on  $^{137}\text{Cs}$  profiles should be readily apparent after 10 years. For example, a  $K_d$  value of  $10^3$  (typical of values derived from tracer experiments and pore water measurements) would result in a 46% decrease in peak  $^{137}\text{Cs}$  activity. The actual decrease in  $^{137}\text{Cs}$  after 10 years is only 20%, exactly that expected for radioactive decay. These results suggest that literature values of  $K_d$  overestimate the mobility of bomb-derived  $^{137}\text{Cs}$  in Skan Bay sediments. This has two important implications for geochemical and radioecological studies in other anoxic, ammonia-rich sediments.

First, sediment geochronologies based on the first appearance of bomb-derived  $^{137}\text{Cs}$  are unlikely to be biased by radionuclide mobility. Second, there appears to be little risk that a significant portion of the sediment pool of bomb-derived  $^{137}\text{Cs}$  will be released to the water column over time periods comparable to the  $^{137}\text{Cs}$  half-life.

(3) Combining multiple tracers and a time series approach provides a powerful tool for elucidating the details of sediment deposition processes. The use of  $^{210}\text{Pb}$  with steady state supply and  $^{137}\text{Cs}$  with highly time-dependent input provides complementary information regarding sedimentation rates and departures from steady-state deposition. The time series approach provides a means to verify anomalous features in sediment profiles and to directly estimate radionuclide mobility.

### Acknowledgments

We thank Chris Martens for use of his laboratory facilities, George Kipphut and Larry Benninger for discussion and counter calibration, and the crew and technical staff of the R/V *Alpha Helix* for sustenance and field assistance. George Kipphut provided the detailed bathymetry of Skan Bay, Susan Henrichs supplied the 1990 ammonium data, and J.K. Cochran, C.A. Nittrouer, and L. Benninger provided critical review. This work was supported in part by NSF grants OCE 84-008674, 85-19534, and 89-17653. Contribution no. 996 from the Institute of Marine Science, University of Alaska.

### References

- Alberts, J.J., Tilly, L.J. and Vigerstad, T.J., 1979. Seasonal cycling of cesium-137 in a reservoir. *Science*, 203: 649-651.
- Alperin, M.J., 1988. The carbon cycle in an anoxic marine sediment: concentrations, rates, isotope ratios, and diagenetic models. Ph.D. Thesis, Univ. Alaska, Fairbanks, 241 pp.
- Alperin, M.J., Reeburgh, W.S. and Devol, A.H., 1992. Organic carbon remineralization and preservation in sediments of Skan Bay, Alaska. In: J.K. Whelan and J.W. Farrington (Editors), *Productivity, Accumulation, and Preservation of Organic Matter in Recent and Ancient Sediments*. Columbia Univ. Press, New York, N.Y., pp. 99-122.
- Beasley, T.M., Carpenter, R. and Jennings, C.D., 1982. Plutonium,  $^{241}\text{Am}$  and  $^{137}\text{Cs}$  ratios, inventories and vertical profiles in Washington and Oregon continental shelf and margin sediments. *Geochim. Cosmochim. Acta*, 46: 1931-1946.
- Brockman, S.R., Espionosa, A.F. and Michael, J.A., 1988. Catalog of intensities and magnitudes for earthquakes in Alaska and the Aleutian Islands—1786-1981. U.S. Geol. Surv. Bull., 1840, 199 pp.
- Brouwer, E., Baeyens, B., Maes, A. and Cremers, A., 1983. Cesium and rubidium ion equilibria in illite clay. *J. Phys. Chem.*, 87: 1213-1219.
- Buchholz, M.R., Santschi, P.H. and Broecker, W.S., 1986. Comparison of radiotracer  $K_D$  values from batch equilibrium experiments with in-situ determinations in the deep-sea using the MANOP lander: The importance of geochemical mechanisms in controlling ion uptake and migration. In: T.H. Sibley and C. Myttenaere (Editors), *Application of Distribution Coefficients to Radiological Assessment Models*. Elsevier, New York, pp. 192-205.
- Chanton, J.P., Martens, C.S. and Kipphut, G.W., 1983. Lead-210 sediment geochronology in a changing coastal environment. *Geochim. Cosmochim. Acta*, 47: 1791-1804.
- Comans, R.N.J. and Hockley, D.E., 1992. Kinetics of cesium sorption on illite. *Geochim. Cosmochim. Acta*, 56: 1157-1164.
- Comans, R.N.J., Middelburg, J.J., Zonderhuis, J., Woittiez, J.R.W., De Lange, G.J., Das, H.A. and Van der Weijden, C.H., 1989. Mobilization of radiocesium in pore water of lake sediments. *Nature*, 339: 367-369.
- Comans, R.N.J., Haller, M. and De Preter, P., 1991. Sorption of cesium on illite: Non-equilibrium behavior and reversibility. *Geochim. Cosmochim. Acta*, 55: 433-440.
- Cremers, A., Elsen, A., De Preter, P. and Maes, A., 1988. Quantitative analysis of radiocesium retention in soils. *Nature*, 335: 247-249.
- Crusius, J. and Anderson, R.F., 1991. Immobility of  $^{210}\text{Pb}$  in Black Sea sediments. *Geochim. Cosmochim. Acta*, 55: 327-333.
- Cutshall, N.H., Larsen, I.L. and Olsen C.R., 1983. Direct analysis of  $^{210}\text{Pb}$  in sediment samples: self-absorption corrections. *Nuclear Instrum. Methods*, 206: 309-312.
- Davidson, C.I., Harrington, J.R., Stephenson, M.J., Monaghan, M.C., Pudykiewicz, J. and Schell, W.R., 1987. Radioactive cesium from the Chernobyl accident in the Greenland ice sheet. *Science*, 237: 633-634.
- Devell, L., Tovedal, H., Bergstrøm, U., Appelgren, A., Chyssler, J. and Andersson, L., 1986. Initial observations of fallout from the reactor accident at Chernobyl. *Nature*, 321: 192-193.
- Duursma, E.K. and Bewers, J.M., 1986. Application of  $K_d$ s in marine geochemistry and environmental assessment. In: T.H. Sibley and C. Myttenaere (Editors), *Application of Distribution Coefficients to Radiological Assessment Models*. Elsevier, New York, pp. 138-165.
- Duursma, E.K. and Eisma, D., 1973. Theoretical, experimental and field studies concerning reactions of radioisotopes with sediments and suspended particles of the sea. Part C: Applications to field studies. *Neth. J. Sea Res.*, 6: 265-324.
- Evans, D.W., Alberts, J.J. and Clark, R.A., III, 1983. Reversible ion-exchange fixation of cesium-137 leading to mobilization from reservoir sediments. *Geochim. Cosmochim. Acta*, 47: 1041-1049.

- Francis, C.W. and Brinkley, F.S., 1976. Preferential adsorption of  $^{137}\text{Cs}$  to micaceous minerals in contaminated freshwater sediments. *Nature*, 260: 511–513.
- Hirschberg, D.J. and Schubel, J.R., 1979. Recent geochemical history of flood deposits in northern Chesapeake Bay. *Estuarine Coastal Mar. Sci.*, 9: 771–784.
- Imboden, D.M. and Stiller, M., 1982. The influence of radon diffusion on the  $^{210}\text{Pb}$  distribution in sediments. *J. Geophys. Res.*, 87: 557–565.
- Kippel, G.W., 1978. An investigation of sedimentary processes in lakes. Ph.D. Thesis, Columbia Univ., New York, 180 pp.
- Koide, M., Bruland, K.W. and Goldberg, E.D., 1973. Th-228/Th-232 and Pb-210 geochronologies in marine and lake sediments. *Geochim. Cosmochim. Acta*, 37: 1171–1187.
- Lerman, A., 1977. Migrational processes and chemical reactions in interstitial waters. In: E.D. Goldberg, I.N. McCave, J.J. O'Brien and J.H. Steele (Editors), *The Sea*. Wiley, New York, 6, pp. 695–738.
- Lerman, A., 1979. *Geochemical Processes: Water and Sediment Environments*. Wiley, New York, 481 pp.
- Levi, B.G., 1986. Soviets assess cause of Chernobyl accident. *Physics Today*, 39(12): 17–20.
- Li, Y.-H. and Gregory, S., 1974. Diffusion of ions in seawater and in deep-sea sediments. *Geochim. Cosmochim. Acta*, 38: 703–714.
- Lisitzin, A.P., 1972. *Sedimentation in the World Ocean*. SEPM Spec. Publ., 17, 218 pp.
- Lomenick, T.F. and Tamura, T., 1965. Naturally occurring fixation of cesium-137 on sediments of lacustrine origin. *Soil Sci. Soc. Proc.*, 29: 383–387.
- Lynch, D.R. and Officer, C.B., 1984. Nonlinear parameter estimation for sediment cores. *Chem. Geol.*, 44: 203–225.
- Murray, J.W., Grundmanis, V. and Smethie, W.M., Jr., 1978. Interstitial water chemistry in the sediments of Saanich Inlet. *Geochim. Cosmochim. Acta*, 42: 1011–1026.
- Nyffeler, U.P., Li, Y.-H. and Santschi, P.H., 1984. A kinetic approach to describe trace-element distribution between particles and solution in natural aquatic systems. *Geochim. Cosmochim. Acta*, 48: 1513–1522.
- Paetzel, M. and Schrader, H., 1992. Recent changes recorded in anoxic Barnesfjord sediments: Western Norway. *Mar. Geol.*, 105: 23–36.
- Patel, B., Patel, S. and Pawar, S., 1978. Desorption of radioactivity from nearshore sediment. *Estuarine Coastal Mar. Sci.*, 7: 49–58.
- Robbins, J.A., 1978. *Geochemical and geophysical applications of radioactive lead*. In: J.O. Nriagu (Editor), *The Biogeochemistry of Lead in the Environment*. Elsevier, Amsterdam, pp. 285–393.
- Santschi, P.H., Li, Y.-H., Adler, D.M., Amdurer, M., Bell, J. and Nyffeler, U.P., 1983. The relative mobility of natural (Th, Pb, and Po) and fallout (Pu, Am, Cs) radionuclides in the coastal marine environment: results from model ecosystems (MERL) and Narragansett Bay. *Geochim. Cosmochim. Acta*, 47: 201–210.
- Sawhney, B.L., 1972. Selective sorption and fixation of cations by clay minerals: A review. *Clays Clay Miner.*, 20: 93–100.
- Schell, W.R. and Sibley, T.H., 1982. Distribution coefficients for radionuclides in aquatic environments. Final Summary Rep. U.S. Nuclear Regulatory Comm., NUREG/CR-1869.
- Sewell, G., 1982. IMSL software for differential equations in one space variable. *IMSL Tech. Rep. Ser.*, 8202, IMSL Inc., Houston, TX, 15 pp.
- Sholkovitz, E.R. and Mann, D.R., 1984. The pore water chemistry of  $^{239,240}\text{Pu}$  and  $^{137}\text{Cs}$  in sediments of Buzzards Bay, Massachusetts. *Geochim. Cosmochim. Acta*, 48: 1107–1114.
- Sholkovitz, E.R., Cochran, J.K. and Carey, A.E., 1983. Laboratory studies of the diagenesis and mobility of  $^{239,240}\text{Pu}$  and  $^{137}\text{Cs}$  in nearshore sediments. *Geochim. Cosmochim. Acta*, 47: 1369–1379.
- Smith, J.N. and Walton, A., 1980. Sediment accumulation rates and geochronologies measured in the Saguenay Fjord using the Pb-210 method. *Geochim. Cosmochim. Acta*, 44: 25–240.
- Solorzano, L., 1969. Determination of ammonia in natural waters by the phenol-hypochlorite method. *Limnol. Oceanogr.*, 14: 799–801.
- Stanners, D.A. and Aston, S.R., 1981. Factors controlling the interactions of  $^{137}\text{Cs}$  with suspended and deposited sediments in estuarine and coastal environments. In: Impacts of Radionuclide Releases into the Marine Environment. Int. Atomic Energy Agency (IAEA) Symp. IAEA-SM-248/141, Vienna, pp. 131–141.
- Sugai, S.F., 1990. Transport and sediment accumulation of  $^{210}\text{Pb}$  and  $^{137}\text{Cs}$  in two southeast Alaskan fjords. *Estuaries*, 13: 380–392.
- Torgersen, T. and Longmore, M.E., 1984.  $^{137}\text{Cs}$  diffusion in the highly organic sediment of Hidden Lake, Fraser Island, Queensland. *Aust. J. Mar. Freshw. Res.*, 35: 537–548.
- Ullman, W.J. and Aller, R.C., 1982. Diffusion coefficients in nearshore marine sediments. *Limnol. Oceanogr.*, 27: 552–556.